Spatio-temporal dynamics of turbulence trapped in geodesic acoustic modes

Spatio-temporal dynamics of turbulence trapped in geodesic acoustic modes

M. Sasaki[1, 2], T. Kobayashi[3], K. Itoh[2, 4], N. Kasuya[1, 2], Y. Kosuga[1, 2], A. Fujisawa[1, 2], and S.-I. Itoh[1, 2]

[1]Research Institute for Applied Mechanics, Kyushu University, Kasuga 816-8580, Japan
[2]Research Center for Plasma Turbulence, Kyushu University, Kasuga 816-8580, Japan
[3]National Institute for Fusion Science, Toki 509-5292, Japan
[4]Institute of Science and Technology Research, Chubu University, Kasugai 487-8501, Japan

Abstract

Spatio-temporal dynamics of turbulence with the interaction of geodesic acoustic modes (GAMs) are investigated, focusing on the phase-space structure of turbulence, where the phase-space consists of real-space and wavenumber-space. Based on the wave-kinetic framework, the coupling equation between the GAM and the turbulence is numerically solved. The turbulence trapped by the GAM velocity field is obtained. Due to the trapping effect, the turbulence intensity increases where the second derivative of the GAM velocity (curvature of the GAM) is negative. While, in the positive-curvature region, the turbulence is suppressed. Since the trapped turbulence propagates with the GAMs, this relationship is sustained spatially and temporally. The dynamics of the turbulence in the wavenumber spectrum is converted in the evolution of the frequency spectrum, and the simulation result is compared with the experimental observation in JFT-2M tokamak, where the similar patterns are obtained. The turbulence trapping effect is a key to understand the spatial structure of the turbulence in the presence of sheared flows.

Keywords: zonal flows, GAMs, turbulence, turbulence trapping

1 Introduction

Interaction between turbulence and sheared flows has been an important subject in studies of magnetically confined plasmas. Theoretical models for turbulence suppression have been proposed such as the suppression due to the flow shear [1] and due to the flow cuvature [2]. Experimental validation for the interaction between sheared flows and turbulence has been reported [3]-[7]. The spatial structure of the energy transfer functions between the turbulence and the zonal flows (ZFs) has been observed in a basic plasma experiment

[8]. In researches on the interaction between ZFs and turbulence, predator-prey model has been widely studied [9]-[13] and applied to experiments [14]-[16]. However, the spatial structure of turbulence within the wavelength of the ZFs can not be predicted by the predator-prey model, since the spatial integral over the wavelength of the ZFs is implicitly performed in the derivation of the model. It should be noted that the wavelength of ZFs is comparable to the scale length of the radial electric field which induces the transport barriers [14]. A model that can predict the spatial structure of turbulence in the presence of shear flows is required.

Turbulence trapping effect can be treated when the phase-space dynamics is considered, where the phase-space consists of real-space and wavenumber-space [17, 18]. Turbulence trapping could have a significant impact on the spatial profile of the turbulence [19]. Therefore, the phase-space dynamics should be considered for the interaction between turbulence and sheared flows. In addition, validation of theoretical models is essential for understanding experimental observations. Geodesic acoustic modes (GAMs) are relatively easy to be observed experimentally, and details of their properties have been reported [20]-[23]. Thus, there is a chance to test models of the interaction between turbulence and sheared flows in the study of GAMs.

In this study, we investigate the phase-space dynamics of turbulence with the interaction of the GAMs, based on the wave-kinetic framework. Spatial structures of the turbulence and the GAMs are obtained, and they are compared with experimental observation. Due to the turbulence trapping by the GAM, the turbulence is accumulated at regions where the curvature of the GAM (spatial-second-derivative of the GAM flow) is negative, and the turbulence is suppressed at the positive curvature region. This phase relation is sustained with the propagation of the GAM. If one observes this relation by a local measurement, the turbulence is observed to increase and decrease when the poloidal flow is in the electron and ion diamagnetic drift directions, respectively. A guideline for identify the turbulence trapping effect is obtained by rewriting this relation for the evolution of the frequency spectrum. This is because simultaneous measurement of the turbulence wavenumber spectrum at different radial locations is still challenging. The simulation results are compared with the experiment, where the similar relation is obtained. The rest of the paper is organized as follows. Model is introduced in section2, and the simulation results are shown in section3. Comparison with the experiment is described in section4. Summary is given in section5.

2 Model

We consider a high aspect ratio, circular cross-section toroidal plasma. The toroidal coordinate (r, θ, ζ) is used, where $\nabla r, \nabla\theta$ and $\nabla\zeta$ are the radial, poloidal and toroidal directions, respectively. The governing equation for the coupling of the turbulence with

the GAM is as follows [9], [28, 29].

$$\partial_t N_k + \frac{\partial \omega_k}{\partial k_r}\nabla_r N_k - k_\theta \nabla_r \tilde{V_\theta}\frac{\partial N_k}{\partial k_r} = \gamma_L N_k - \Delta\omega N_k^2, \tag{1}$$

$$\partial_t \tilde{V_\theta} + 2\epsilon^2 R\langle \tilde{n}\sin\theta\rangle = -\nabla_r \Pi_{r\theta} + \mu_G \nabla_r^2 \tilde{V_\theta}, \tag{2}$$

$$\partial_t \tilde{n} - \frac{2}{R}\tilde{V_\theta}\sin\theta + \nabla_\parallel \tilde{V_\parallel} = -\nabla_r \Gamma_r, \tag{3}$$

Here, time and space are normalized by $\rho_s^{-1}V_d$ and ρ_s, where ρ_s is the ion sound gyro-radius and V_d is the diamagnetic drift velocity, respectively. The normalized action of the turbulence is denoted by N_k, and ω_k is the frequency of the turbulence, where N_k is a function of r and the wavenumbers, k_r and k_θ. The linear growth rate and the nonlinear decorrelation rate of turbulence are denoted by γ_L and $\Delta\omega$, respectively. The GAM fluctuations of the poloidal and parallel flows and the density are denoted by $\tilde{V_\theta}, \tilde{V_\parallel}$ and $\tilde{n}$, respectively. The geometry factor ϵ is defined as $\epsilon = L_n/R$, where L_n is the density scale length and R is the major radius. The GAM is coupled with the turbulence via the turbulence driven Reynolds stress $\Pi_{r\theta}$ and the particle flux Γ_r. The viscosity for the GAM, μ_G, is introduced. We consider the drift wave type turbulence. Thus, ω_k and N_k are given as

$$\omega_k = \frac{k_\theta}{1 + k_r^2 + k_\theta^2} + k_\theta \tilde{V_\theta}, \tag{4}$$

$$N_k = \left(1 + k_r^2 + k_\theta^2\right)^2 |\phi_k|^2, \tag{5}$$

where ϕ_k is the normalized turbulent electrostatic potential. The turbulence frequency ω_k includes the doppler shift due to the GAM velocity. The Reynolds stress can be given as

$$\Pi_{r\theta} = -\int \frac{k_r k_\theta}{\left(1 + k_r^2 + k_\theta^2\right)^2} N_k d^2k. \tag{6}$$

We focus on plasmas with high safety factor $q \gg 1$ and weak magnetic shear. In this case, the return flow effect, which comes from the parallel compression, the third term in the left hand side of Eq. (3), can be neglected. Note that this term is important for the low frequency zonal flow, where the effective inertia is enhanced by a factor $1 + 2q^2$ [30, 31]. In addition, the contribution from the particle transport modulation (dynamics shearing, the right hand side of Eq. (3)) can be ignored in the low magnetic shear case [28]. In order to simplify the situation, we use the slab coordinate x instead of r, hereafter. In this situation, the GAM evolution can be obtained as

$$\partial_t^2 \tilde{V_\theta} + \omega_G^2 \tilde{V_\theta} = -\partial_x \partial_t \Pi_{x\theta} + \mu_G \partial_x^2 \partial_t \tilde{V_\theta}, \tag{7}$$

where the GAM frequency is defined as $\omega_G = \sqrt{2}\epsilon$, which corresponds to $\sqrt{2}c_s/R$ in the dimensional form.

In the conventional theories for the interaction of ZFs with turbulence [9], the predator-prey model is deduced from the linear response of N_k. In the derivation of the predator-prey model, the spatial integration within the ZFs wavelength is used. Thus, the predator-prey model, including its extension for the one-dimensional model [11], can not predict

the spatial structures of the turbulence within the scale of the ZFs wavelength. In this study, we investigate the spatial structure of the turbulence, by considering the phase-space dynamics of the turbulence, where the evolution of the GAM is calculated without any assumptions for the evaluation of the Reynolds stress within the framework of the wave-kinetic theory.

The coupling equations, Eqs. (1) and (7), are calculated numerically. The dynamics of the turbulence in (x, k_r)-space is simulated. The simulation conditions are as follows. A spatially homogeneous turbulence is assumed, where γ_L and $\Delta\omega$ are given constant in space. The wavenumber-dependence of γ_L is given as $\gamma_L = \gamma_0 \exp\left(-(k_r - k_0)^2/\Delta k^2\right)$. The poloidal wavenumber k_θ is conserved in the interaction with the GAMs, so that the k_θ is given as a parameter. The parameters are chosen to be $\gamma_0 = 0.5, \Delta\omega = 1.5, k_0 = 0.3, \Delta k = 1, k_\theta = 1, \omega_G = 0.1, \mu_G = 0.1$. The periodic boundary condition for the x-direction is used. The perturbation is introduced to the turbulence as the initial condition, and the time evolution of the turbulence and the GAM are investigated.

3 Spatial-temporal relation between GAMs and turbulence

In this section, we describe the simulation results on the spatio-temporal structures of the GAM and the turbulence.

The nonlinear saturated state is obtained by solving Eqs. (1) and (7). The time evolution of the energy is shown in Fig. 1, where the energies of the GAM and turbulence are defined as $\mathcal{E}_{GAM} = \int |V_\theta|^2 dx$ and $\mathcal{E}_{turb} = \int \left(1 + k_r^2 + k_\theta^2\right)^{-1} N_k dx dk_r$, respectively. The turbulence energy is reduced when the energy of the GAM becomes large. The spatio-temporal patterns of the GAM velocity and the turbulence at the saturated state are shown in Fig. 2. The GAM propagates in the x-direction monotonically. The turbulence intensity also has the similar pattern with the GAM; the region where the turbulence is suppressed propagates with the GAM. The phase relation between the modulated turbulence intensity and the GAM is sustained with the propagation of the GAM.

The snapshots of the turbulence N_k in the phase-space are shown in Fig. 3, in which the initial condition and the saturated state are shown. At $t = 0$, a small perturbation is applied to the spatially homogeneous turbulence, and the perturbation evolves to form the GAM structure. Note that the nonlinear saturated state is independent on the pattern of initial conditions. At the nonlinear saturated state, the turbulence is trapped in the GAM velocity, and their phase relation is sustained spatially and temporally. Thus, the trapped turbulence propagates with the phase velocity of the GAM. Due to the trapping, the turbulence is accumulated where the second derivative of the GAM velocity field is negative, $\partial_x^2 V_\theta < 0$, [19]. While, in the region of $\partial_x^2 V_\theta > 0$, the turbulence is suppressed. If one observes this system by a local measurement, like a Langmuir probe or heavy ion beam probe (HIBP) [20, 21], one can see that the turbulence decreases when the GAM velocity is in the ion-diamagnetic drift direction, and increases when the GAM velocity is in the electron-diamagnetic drift direction. This property could be a guideline to identify the island structure in the phase space.

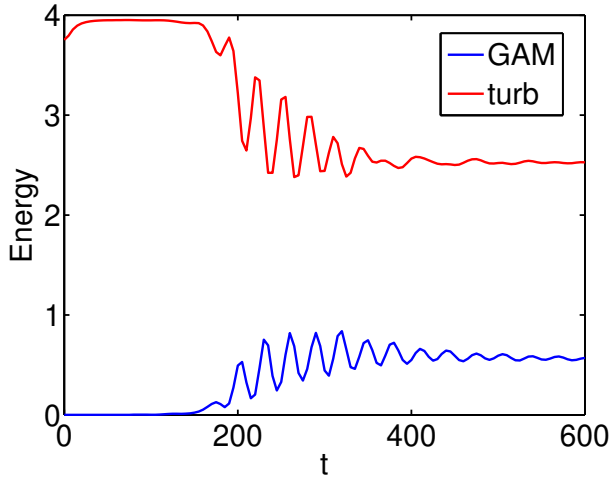

Fig. 1: Time evolution of the energies of the GAM and turbulence.

The mechanism of the turbulence trapping can be explained as follows [17]-[19]. The wave-kinetic equation, Eq. (1), can be written by using the Poisson bracket as

$$\partial_t N_k + \{\omega_k, N_k\} = \gamma_L N_k - \Delta\omega N_k^2. \tag{8}$$

One can see that ω_k is the constant of motion in the case when $\gamma_L = 0, \Delta\omega = 0$. The turbulence frequency, ω_k, corresponds to the characteristics of Eq. (1), in the same way that, for example, the Hamiltonian for the plasma particles corresponds to the characteristics of the Vlasov equation. Thus, the turbulence moves along the contour of ω_k. When the sheared flow exists, the contour of ω_k is deformed by the doppler-shift to form the island structure in the phase space, as shown by the white lines in Figs. 3(a) and (b). Here, the island width Δk can be estimated by using Eq. (4) as

$$\Delta k = \sqrt{\frac{(1+k_\theta^2)^2 V_G}{1-(1+k_\theta^2)^2 V_G}}, \tag{9}$$

where V_G is the amplitude of V_θ. As the turbulence moves along the contour of ω_k, the turbulence in the region $|k_r| < \Delta k$ is trapped in the GAM, which propagates with the phase velocity of the GAM. Here, the separatrix of the island in the phase space corresponds to the region where the curvature of the GAM is positive. Therefore, the turbulence is suppressed/accumulated in the positive/negative curvature region.

In order to clarify the spatial structure of the energy transfer between the GAM and the turbulence, the energy equations are discussed here. The energy equations of the

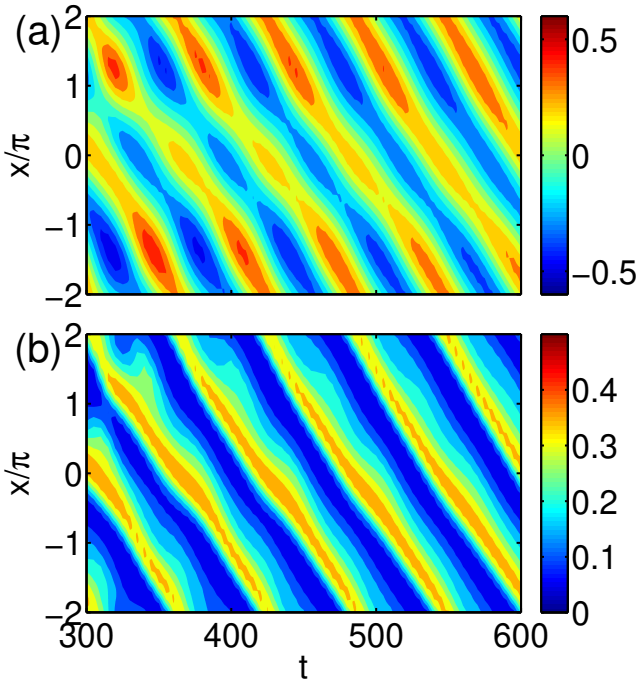

Fig. 2: Spatio-temporal patterns of (a) GAM velocity and (b) turbulence intensity.

GAM and the turbulence are obtained from Eqs. (1), and (2) as

$$\partial_t I + \partial_x \left(\hat{v}_g I\right) = W_{turb} + \hat{\gamma}_L I - \Delta\hat{\omega} I^2, \tag{10}$$

$$\partial_t \tilde{V_\theta}^2 = W_G + 2\mu_G \tilde{V_\theta} \partial_x^2 \tilde{V_\theta}, \tag{11}$$

where I is the energy density of the turbulence defined as $I(x,t) = \int \left(1 + k_r^2 + k_\theta^2\right)^{-1} N_k dk_r$, and the terms, $\hat{v}_g I, \hat{\gamma}_L I$ and $\Delta\hat{\omega}$, are given as

$$\hat{v}_g I = \int v_g \left(1 + k_r^2 + k_\theta^2\right)^{-1} N_k dk_r, \tag{12}$$

$$\hat{\gamma}_L I = \int \gamma_L \left(1 + k_r^2 + k_\theta^2\right)^{-1} N_k dk_r, \tag{13}$$

$$\Delta\hat{\omega} I^2 = \int \Delta\omega \left(1 + k_r^2 + k_\theta^2\right)^{-1} N_k^2 dk_r. \tag{14}$$

Here, the effective linear growth rate and nonlinear decorrelation rate are denoted by $\hat{\gamma}_L$ and $\Delta\hat{\omega}$, respectively. The energy exchange rates between the GAM and the turbulence,

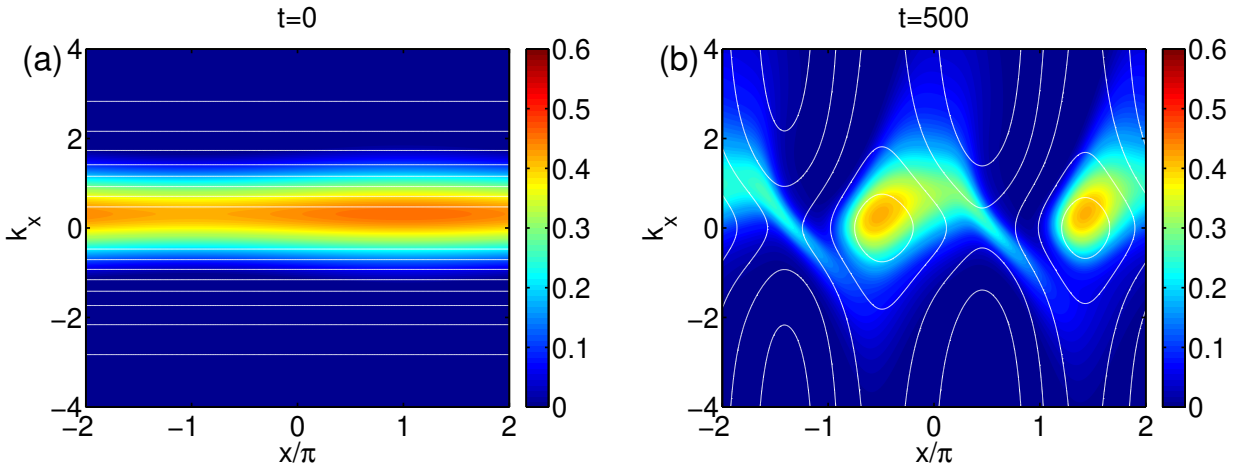

Fig. 3: Snapshots of action of turbulence, $N_k(x, k_r)$, in the phase-space. (a) The initial condition and (b) the nonlinear saturated state are shown. The white contour corresponds to that of ω_k.

W_G and W_{turb}, are obtained as

$$W_{turb} = \left[\int \frac{2k_r k_\theta}{(1 + k_r^2 + k_\theta^2)^2} N_k dk_r \right] \partial_x \tilde{V}_\theta = -2\Pi_{x\theta} \partial_x \tilde{V}_\theta, \tag{15}$$

$$W_G = -2\tilde{V}_\theta \partial_x \Pi_{x\theta}. \tag{16}$$

The spatial profiles of the energy transfer functions, W_{turb} and W_G, are different with each other. Namely, the region where the GAM obtains energy from the turbulence is different from the region where the turbulence loses energy. It should be noted that the net exchange energy between the GAM and the turbulence is conserved, $\int (W_G + W_{turb}) dx = 0$.

We describe the spatial profiles of the energy equation for the turbulence, which are calculated from the simulation result. The spatial relationship between the phase-space structure of N_k and the turbulent force is shown in Figs. 4(a) and (b), where the turbulent force is defined as the radial derivative of the Reynolds stress, $-\partial_x \Pi_{x\theta}$. The turbulent force has a highly nonlinear waveform, where it has steep gradient. The spatial profiles of the energy transfer functions, W_G and W_{turb}, are plotted in Fig. 4 (c). The positive W_G can be seen in the regions where the GAM velocity has a curvature, which indicates that the GAM obtains energy from the turbulence. While, the negative W_{turb} is obtained in the regions where the GAM has a shear, which implies that the energy of the turbulence is reduced there. The profile of the propagation effect of the turbulence, the second term

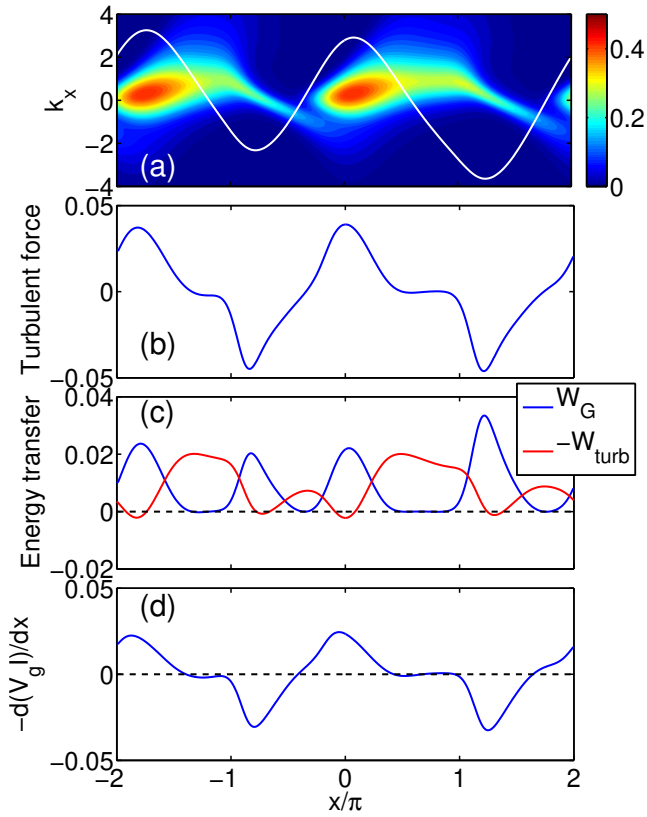

Fig. 4: Spatial pattern of turbulent driving force. (a) Snapshots of N_k and $\tilde{V_\theta}$ at $t = 600$, (b) turbulent force $-\partial_x \Pi_{x\theta}$, (c) Energy transfer functions between GAM and turbulence, and (d) turbulence propagation term (the second term in LHS of Eq. (10)).

in left hand side (LHS) of Eq. (10), is shown in Fig. 4 (d). This term strongly reflects the effect of the trapping. The magnitude of this term is the same order with the energy transfer functions, so that the turbulence propagation is also important for determining the turbulence profile. It is noted that the predator-prey model can be obtained by integrating Eqs. (10) and (11) [9]. By the spatial integration, the turbulence propagation effect, the second term in LHS of Eq. (10), disappears. Although the energy exchange term, W_{turb} and W_G, are important for determining the spatially integrated energies of the turbulence, the turbulence propagation effect (turbulence trapping effect) is important for determining the spatial profile as well as the energy exchange term.

4 Comparison with experimental observation

This relationship of the turbulence with the GAM can be described in the real-space and frequency-space. This is because the simultaneous measurement of the wavenumber spectrum of the turbulence at different radial locations is still challenging. The turbulence we consider here is the drift wave, so that it follows the dispersion relation as shown

in Eq. (4). Using the dispersion relation, the k_r-spectrum can be interpreted in the frequency-space, as $N_k(x, k_r) \to N_k(x, \omega)$. The transformation of $N_k(x, k_r)$ to $N_k(x, \omega)$ is possible by the following reason. In the framework of the wave-kinetic theory, the turbulence poloidal wavenumber k_θ is constant in time and space in the interaction with the GAM, while k_r changes spatially and temporally, in the limit that the growth and nonlinear damping of turbulence are absent [18, 19]. This is because the deformation of the turbulence wavenumber in the radial (poloidal) direction is due to the radial (poloidal) inhomogeneity of the doppler shift by the sheared flow, where we do not consider the poloidal inhomogeneity of the GAM velocity field. Thus, the change of the turbulence frequency is only due to the change of k_r. Figure 5(a) illustrates the time evolution of $N_k(x, \omega)$ at $x = 0$. The trapped turbulence also forms island structures in the frequency spectrum.

This simulation results are compared with an experiment in JFT-2M tokamak. In this experiment, an HIBP is used to observe the interaction of the GAMs and turbulence [20, 32], where the turbulence was identified as the drift wave [30]. Wavelet analysis is performed to obtain the evolution of the turbulence spectrum. Figure 5(b) illustrates the time evolutions of the poloidal velocity of the GAM component and the frequency spectrum of the turbulence, where these time evolutions are obtained at the same location. Increase of the turbulent intensity is in phase of the GAM velocity. This characteristic is similar to the simulation. The turbulence modulated by the GAM show the island structure in the frequency spectrum, and its relation is sustained during the period that the GAM exists. The detailed spatio-temporal patterns are described in [32]. The turbulence trapping effect is a key to understand the spatial structure of the turbulence in the presence of sheared flows.

5 Summary

Spatial structures of GAMs and turbulence is investigated, focusing on the phase-space structure of turbulence. Based on the wave-kinetic equation, the interaction between the GAM and the turbulence is investigated. The turbulence trapped by the GAM velocity field is obtained in the real-wavenumber space. Due to the trapping effect, the turbulence intensity increases where the second derivative of the GAM velocity is negative, $\partial_x^2 V_\theta < 0$. While, in the region of $\partial_x^2 V_\theta > 0$, the turbulence is suppressed. Since the trapped turbulence propagates with the GAMs, this relationship is sustained spatially and temporally. Namely, the turbulence intensity increases and decreases when the GAM velocity is in the electron and ion diamagnetic drift direction, respectively. This relation is interpreted for the evolution of the frequency spectrum, and the simulation result is compared with the experimental observation in JFT-2M tokamak. The similar spatio-temporal pattern is obtained. The turbulence trapping effect is a key to understand the spatial structure of the turbulence in the presence of sheared flows.

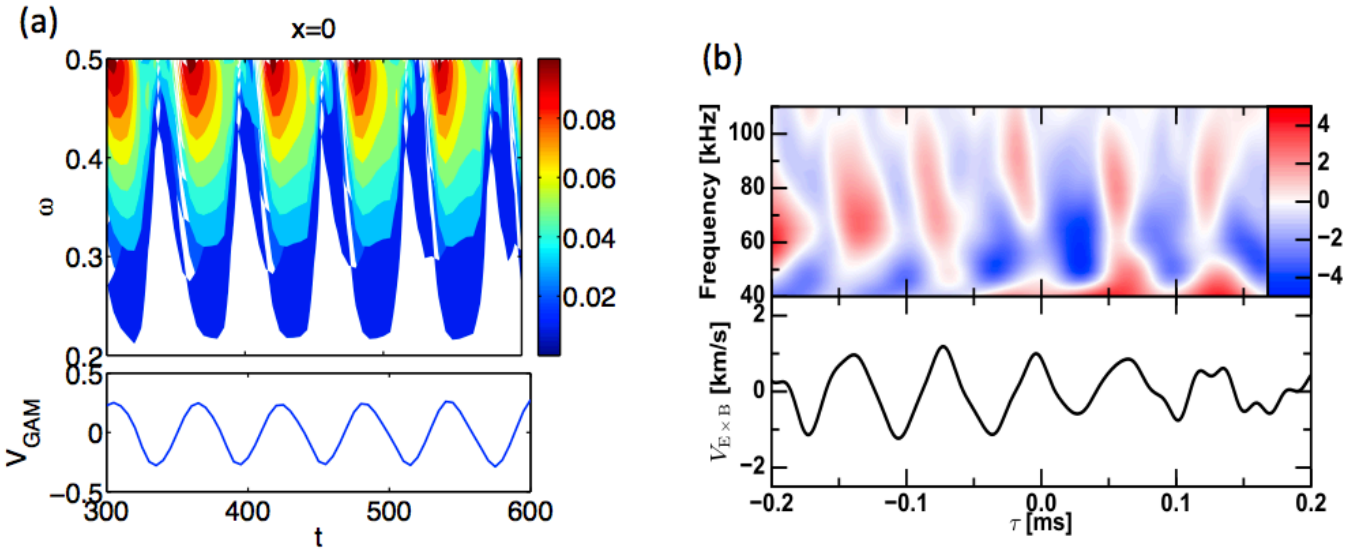

Fig. 5: Time evolution of frequency spectrum of turbulence and the GAM. (a) Simulation result and (b) experimental observation are shown.

Acknowledgement

This work was partly supported by a grant-in-aid for scientific research of JSPS, Japan (15H02155, 16K18335, 16H02442, 17H06089) and by the collaboration programs of NIFS (NIFS15KNST089, NIFS17KNST122) and of the RIAM of Kyushu University.

References

[1] H. Biglari, P. H. Diamond, P. W. Terry, Phys. Plasmas, **2**, 1 (1990).

[2] K. Itoh, S.-I. Itoh, K. Kamiya, N. Kasuya, Plasma Phys. Control. Fusion, **57**, 075008 (2015).

[3] T. Tokuzawa, S. Inagaki, K. Ida, K. Itoh, T. Ido, A. Shimizu, H. Takahashi, S. Kitajima, N. Tamura, M. Yoshinuma, H. Tsuchiya, I. Yamada, K. Tanaka, T. Akiyama, Y. Nagayama, K. Kawahata, K. Y. Watanabe, H. Yamada, and LHD Experiment Group, Phys. Plasmas, **21**, 055904 (2014).

[4] T. Tokuzawa, Nucl. Fusion, **57**, 025001 (2017).

[5] K. Kamiya, K. Itoh, S.-I. Itoh, Sci. Rep., **16**, 30585 (2016).

[6] T. A. Carter, J. E. Maggs, Phys. Plasmas, **16**, 012304 (2009).

[7] T. Kobayashi, K. Itoh, T. Ido, K. Kamiya, S.-I. Itoh, Y. Miura, Y. Nagashima, A. Fujisawa, S. Inagaki, K. Ida, submitted to Sci. Rep. (2017).

[8] P. Mantz, M. Xu, N. Fedorczak, G. R. Tynan, Phys. Plasmas **19**, 012309 (2012).

[9] P. H. Diamond, S.-I. Itoh, K. Itoh, T. S. Hahm, Plasma Phys. Control. Fusion, **47**, R35 (2005).

[10] K. Miki, P. H. Diamond, Nucl. Fusion, **51**, 103003 (2011).

[11] K. Miki, P. H. Diamond, S.-H. Hahn, W. W. Xiao, O. D. Gurcan, G. R. Tynan, Phys. Rev. Lett., **110**, 195002 (2013).

[12] M. Sasaki, K. Itoh, A. Ejiri, Y. Takase, Plasma Phys. Control. Fusion, **51**, 085002 (2009).

[13] M. Sasaki, K. Itoh, S.-I. Itoh, N. Kasuya, Nucl. Fusion, **52**, 023009 (2012).

[14] L. Schmitz, L. Zeng, T. L. Rhodes, J. C. Hillesheim, E. J. Doyle, R. J. Groebner, W. A. Peebles, K. H. Burrell, G. Wang, Phys. Rev. Lett., **108**, 155002 (2012).

[15] Z. Yan, G. R. McKee, R. Fonck, P. Gohil, R. J. Groebner, T. H. Osborne, Phys. Rev. Lett., **112**, 125002 (2014).

[16] G. R. Tynan, M. Xu, P. H. Diamond, J. A. Boedo, I. Cziegler, N. Fedorczak, P. Manz, K. Miki, S. Thakur, L. Schmitz, L. Zeng, E. J. Doyle, G. M. McKee, Z. Yan, G. S. Xu, B. N. Wan, H. Q. Wang, H. Y. Guo, J. Dong, K. Zhao, J. Cheng, W.Y. Hong, L.W. Yan, Nucl. Fusion, **53**, 073053 (2013).

[17] P. Kaw, K. Mima, K. Nishikawa, Phys. Rev. Lett. **34**, 803 (1975).

[18] P. Kaw, R. Singh, P. H. Diamond, Plasma Phys. Control. Fusion, **44**, 51 (2002).

[19] M. Sasaki, K. Itoh, K. Hallatschek, N. Kasuya, M. Lesur, Y. Kosuga, S.-I. Itoh, Sci. Rep. **7**, 16767 (2017).

[20] T. Ido, Y Miura, K Kamiya, Y Hamada, K Hoshino, A Fujisawa, K Itoh, S-I Itoh, A Nishizawa, H Ogawa, Y Kusama, JFT-2M group, Plasma Phys. Control. Fusion, **48**, S41 (2006).

[21] Y. Nagashima, K. Hoshino, A. Ejiri, K. Shinohara, Y. Takase, K. Tsuzuki, K. Uehara, H. Kawashima, H. Ogawa, T. Ido, Y. Kusama, Y. Miura, Phys. Rev. Lett. **95**, 095002 (2005).

[22] A. V. Melnikov, V. A. Vershkov, L. G. Eliseev, S. A. Grashin, A. V. Gudozhnik, L. I. Krupnik, S. E. Lysenko, V. A. Mavrin, S. V. Perfilov, D. A. Shelukhin, S. V. Soldatov, M. V. Ufimtsev, A. O. Urazbaev, G. Van Oost, L. G. Zimeleva, Plasma Phys. Control. Fusion, **48**, S87 (2006).

[23] G. D. Conway, B. Scott, J. Schirmer, M. Reich, A. Kendl, the ASDEX Upgrade Team, Plasma Phys. Control. Fusion, **47**, 1165 (2005).

[24] G. D. Conway, C. Troster, B. Scott, K. Hallatschek, the ASDEX Upgrade Team, Plasma Phys. Control. Fusion, **50**, 055009 (2008).

[25] G. R. MacKee, D. K. Gupta, R. J. Fonck, D. J. Schlossberg, M. W. Shafer, P Gohil, Plasma Phys. Control. Fusion, **48**, S123 (2006).

[26] K. J. Zhao, T. Lan, J. Q. Dong, L. W. Yan, W. Y. Hong, C. X. Yu, A. D. Liu, J. Qian, J. Cheng, D. L. Yu, Q. W. Yang, X. T. Ding, Y. Liu, C. H. Pan, Phys. Rev. Lett. **96**, 255004 (2006).

[27] A. Kramer-Flecken, S. Soldatov, H. R. Koslowski, O. Zimmermann (TEXTOR Team), Phys. Rev. Lett. **97**, 045006 (2006).

[28] K. Itoh, K. Hallatschek, S.-I. Itoh, Plasma Phys. Control. Fusion, **47**, 451 (2005).

[29] A. B. Hassam, J. F. Drake, Phys. Plasmas, **5**, 4002 (1993).

[30] T. Kobayashi, K. Itoh, T. Ido, K. Kamiya, S.-I. Itoh, Y. Miura, Y. Nagashima, A. Fujisawa, S. Inagaki, K. Ida, K. Hoshino, Phys. Rev. Lett. **111**, 035002 (2013).

[31] K. Itoh, S.-I. Itoh, Plasma Phys. Control. Fusion, **38**, 1 (1996).

[32] T. Kobayashi, M. Sasaki, T. Ido, K. Kamiya, Y. Miura, Y. Nagashima, K. Ida, S.-I. Itoh, K. Itoh, to be submitted to Phys. Rev. Lett. (2017).